Neuron
Article

A Motion Direction Preference Map in Monkey V4

Peichao Li,[1,2] Shude Zhu,[1,2] Ming Chen,[1] Chao Han,[1] Haoran Xu,[1] Jiaming Hu,[1] Yang Fang,[1] and Haidong D. Lu[1,*]
[1]Institute of Neuroscience and State Key Laboratory of Neuroscience, Shanghai Institutes for Biological Sciences, Chinese Academy of Sciences, Shanghai 200031, China
[2]These authors contributed equally to this work
*Correspondence: haidong@ion.ac.cn
http://dx.doi.org/10.1016/j.neuron.2013.02.024

SUMMARY

In the primate visual system, area V4 is located in the ventral pathway and is traditionally thought to be involved in processing color and form information. However, little is known about its functional role in processing motion information. Using intrinsic signal optical imaging over large fields of view in V1, V2, and V4, we mapped the direction of motion responses in anesthetized macaques. We found that V4 contains direction-preferring domains that are preferentially activated by stimuli moving in one direction. These direction-preferring domains normally occupy several restricted regions of V4 and tend to overlap with orientation- and color-preferring domains. Single-cell recordings targeting these direction-preferring domains also showed a clustering, as well as a columnar organization of V4 direction-selective neurons. These data suggest that, in contrast to the classical view, motion information is also processed in ventral pathway regions such as area V4.

INTRODUCTION

In the primate visual system, visual information is processed along two parallel pathways: the dorsal visual pathway (projecting from V1–MT–MST) and the ventral visual pathway (projecting from V1–V2–V4–IT) (Mishkin et al., 1983). Consistent with this parallel processing scheme, the majority of neurons in V4 tend to encode object-related information, including color, orientation, depth, and shape (Roe et al., 2012). However, neurons selective for direction of motion have also been found in V4; for example, in macaque monkeys (Zeki 1978) and in owl monkeys (Baker et al., 1981). Estimates of the proportion of directional neurons in the V4 range from 13% (Desimone and Schein, 1987) to 33% (Mountcastle et al., 1987; Ferrera et al., 1994b), which is similar to that in V1 (20%–30%; Orban et al., 1986) or V2 (~15%; Levitt et al., 1994). Also, considering that area V4 is many times larger than area MT (Felleman and Van Essen 1991), the number of directional neurons in these two areas may be comparable. It is not known how these V4 directional neurons are distributed or whether they have a functional organization. Functionally, V4 also seems to be involved in the processing of visual motion information. For example, many V4 neurons were selective to the orientation of motion-defined forms (Mysore et al., 2006). When motion was used as a cue for object discrimination, one fourth of V4 neurons showed significant motion-cue-dependent modulation (Ferrera et al., 1994b). In monkey functional magnetic resonance imaging (fMRI) studies, area V4 was preferentially activated by moving stimuli (Vanduffel et al., 2001) or by changes in the direction of motion (Tolias et al., 2001). All of these suggest that V4 plays a role in motion processing (also see Ferrera and Maunsell, 2005). As V4 is traditionally viewed as a color/form processing center, it is important to know whether motion-related neurons play a functional role in this area.

While the detailed functional structures of early visual cortex have been extensively studied, the functional organization of V4 is not well understood. Early single-cell recording studies have shown that V4 neurons that respond to similar features are often clustered together (Kotake et al., 2009; Tanaka et al., 1986; Watanabe et al., 2002; Yoshioka and Dow, 1996). Recent fMRI studies have revealed color-preferring regions (globs) and orientation-selective regions (interglobs) in V4 (Conway et al., 2007). Consistent with these fMRI findings, optical imaging studies have revealed segregated maps for orientation preference and color preference in V4 (Tanigawa et al., 2010). An early optical imaging study (Ghose and Ts'o, 1997) suggested that orientation preference maps in V4 only exist in foveal regions. A recent study (Tanigawa et al., 2010) has also revealed orientation preference and color preference maps in the central visual field. For study of the functional organization of V4 in peripheral regions, as well as for evaluation of the overall relationship among different cortical features (e.g., retinotopy, preference for orientation and color, preference for motion direction), imaging a significant region of cortex using a large field of view is necessary.

In the present report, we have studied the functional organization of direction-preferring responses in V4 with optical imaging and map-guided single-cell recording in the macaque. We discovered functional domains in V4 that are specifically activated by a single direction of motion. Single-cell recordings confirmed the clustering of directional neurons into separate domains with a columnar organization. The existence of direction-preferring organization in V4 suggests that, in addition to color and form, motion information is also processed in area V4.

RESULTS

Intrinsic signal optical imaging was performed to image cortical responses to drifting gratings in anesthetized and paralyzed macaque monkeys. Population responses of V1, V2, and V4 to

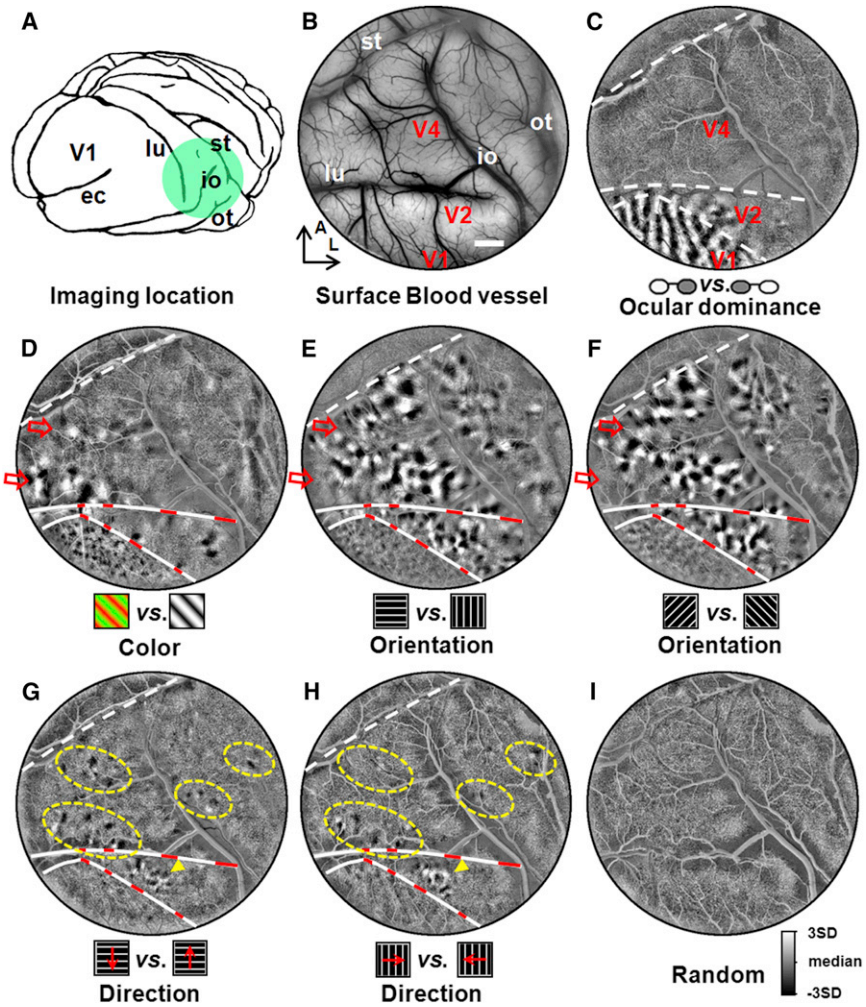

Figure 1. Functional Maps in V4

(A) A schematic of the macaque brain showing the imaging region (green circle) and sulcus locations. lu, lunate; st, superior temporal; ec, external calcarine sulcus; io, inferior occipital sulcus; ot, occipitotemporal.

(B) In vivo image of the blood vessel pattern of the imaging region, ~20 mm diameter. A, anterior; L, lateral. Scale bar, 2 mm.

(C–I) Functional maps (t-maps) obtained with optical imaging. Icons below each map indicate stimulus conditions and statistical comparisons (paired t test, two tailed). Dotted lines indicated area boundaries between V1, V2, and V4. (C) shows an ocular dominance map showing ocular dominance columns in V1. (D) shows a color preference map obtained by comparing isoluminant red-green and achromatic gratings. Red arrows point to color-preferring domains in V4. Short red bars on V2 borders indicate approximate thin stripe locations that are preferentially activated by color stimuli. The same red bars are transferred to maps (E)–(H). (E) and (F) show a 0°-versus-90° orientation preference map (E) and a 45°-versus-135° orientation preference map (F). Color preference regions in V4 (red arrows) and V2 (red bars) have weak orientation selectivity (gray pixels). (G) and (H) show a down-versus-up direction preference map (G) and a right-versus-left direction preference map (H). Yellow dashed ovals outline clusters of direction-preferring domains in V4 (small black and white patches). Yellow arrowhead indicates a direction preference map in V2. (I) shows a condition-randomized map obtained by randomly swapping in half of the rightward motion and leftward motion trials; same data set as in (H). No significant domains are observed in this map. Scale bar in (B) also applies to (C)–(I). See Figures S1, S2, and S3.

different directions of movement were compared. Based on the image maps, neurons inside and outside of V4 direction-preferring domains were recorded and characterized. A total of eight hemispheres were imaged, three of which were further studied using single-unit recordings.

Direction Preference Maps in V4

We used a large craniotomy and cover glass (24 mm diameter) for imaging, which allowed us to include areas V1, V2, and V4 in the same field of view. Figure 1 shows imaging results from Case 1 (right hemisphere). Figure 1A illustrates the imaging field of view (green circle) using the main sulci as landmarks. Figure 1B shows an image of the surface vessel pattern of the selected area. Area V4 exposed on the surface was identified based on sulcal features (Van Essen and Zeki, 1978): anterior to the lunate sulcus and posterior to the superior temporal sulcus. The medial extent of the imaged field of view was approximately 22–23 mm from the midline, and the lateral extent of the field overlies the region surrounding the inferior occipital sulcus where the foveal representation is found (Gattass et al., 1988). Using single horizontal or vertical bars, we obtained a coarse retinotopic map of the exposed V4 area. It is notable that, even with large-field imaging, we could only image about 6°–9° of V4 (Figure S1 available online). Based on the sulcal pattern, it is possible that the most lateral extent of our imaging window encroached upon superior visual fields (Gattass et al., 1988). There are no published images of the functional organization in this foveal region of V1, V2, and V4 in the macaques. In each case, basic functional maps were obtained, including maps for ocular dominance, orientation preference, and color preference. Functional maps in Figures 1C–1I were imaged from the same cortical region in a single imaging session. Each of these maps is a t-value map (t-map), which compares two stimulus conditions (illustrated below each map). T-maps are similar to traditional subtraction maps (e.g., for A versus B t-map, dark pixels are preferentially activated by stimulus A; and white pixels are preferentially activated by stimulus B). Each pixel value is a paired t value obtained by comparing the pixel's response to two stimulus conditions (see Experimental Procedures for additional details). Unlike simple subtraction maps, which only use the mean pixel values, t-maps take into account trial-to-trial variations and thus are a more reliable indicator of significant response than are subtraction maps (see Figure S2 for a comparison of these two types of maps). The V1/V2 border (the lower dotted line in Figure 1C) was

revealed by imaging ocular dominance in V1 using left eye versus right eye stimulation. Thus, based on ocular dominance imaging and sulcal locations, we were able to define the extents of V1, V2, and V4 within the imaging field of view.

To examine the functional organization of neurons responding to color and orientation, we mapped color preference by comparing color versus luminance conditions (Figure 1D) and orientation preference by comparing orthogonal orientation conditions (Figures 1E and 1F). We found color and orientation preference maps in all three areas (V1, V2, and V4). In V1, the color blob pattern (lower left area in Figure 1D) is similar to what has been previously described (Lu and Roe, 2008). The orientation preference map in V1 (lower area of Figures 1E and 1F) is apparent but is relatively weak, perhaps due to the spatial parameters of the stimuli. In V2, color-responsive regions only occupy restricted regions (Figure 1D, short red lines on V1/V2 border and lunate lines). Orientation-preferring domains are seen throughout the mediolateral extent but are punctuated by locations of poor orientation preference regions, which overlie regions of strong color preference. Such complementary color and orientation preference maps are consistent with previous findings in macaque monkeys (Roe and Ts'o, 1995; Lu and Roe, 2008).

In V4, the color preference map is apparent but seems to exhibit a more limited coverage (red arrows in Figure 1D). In this case, there appear to be two large bands: a prominent one close to the lunate sulcus and, more anteriorly, another narrower band. The two orientation preference maps (0° versus 90° and 45° versus 135°; Figures 1E and 1F) exhibit similar coverage throughout the imaged V4 region. Medial to the inferior occipital sulcus, these orientation preference maps appear to form large bands running in a roughly mediolateral direction. Qualitatively, the orientation- and color-preferring regions we observe in V4 appear to be grossly complementary in location, which is consistent with a previous study in the macaque V4 (Tanigawa et al., 2010). The red arrows in Figures 1E and 1F are transferred from Figure 1D and indicate V4 regions having strong color preference but weak orientation preference. We found that the color- and orientation-preferring domains in V4 are of comparable size; the average diameter of a single domain is 527 ± 32 μm (all such expressions are mean ± SEM in this article; n = 25) for the color-preferring domains and 542 ± 17 μm (n = 73) for the orientation-preferring domains, similar to previous observations (Tanigawa et al., 2010).

To test directional preference, we imaged cortical responses to full-field drifting square-wave gratings (0.13° white + 0.53° black for each cycle, speed = 5.33°/s). We tested eight different directions with 30–50 repeats each. Direction preference maps were obtained by comparing two stimulus conditions having opposite directions; a total of four direction preference maps were obtained from eight directions. Two representative direction preference maps from Case 1 are shown in Figure 1G (down versus up) and in Figure 1H (right versus left). Consistent with previous findings (Lu et al., 2010), direction-preferring domains were observed in V2 (yellow arrowhead). It is surprising that, in V4, we also observed clusters of small direction-preferring domains (black or white domains in yellow ovals in Figures 1G and 1H). These domains appeared to be quite small (361 ± 13 μm, n = 44), compared to the V4 orientation- and color-preferring domains mentioned previously. Direction-preferring domains, revealed by different direction comparisons (Figures 1G versus 1H), are mainly located in the same restricted regions. Some small local differences were also observed. For example, some regions, which have domains responding to an up or down direction, have weak left or right direction-preferring domains nearby (e.g., top-left oval in Figure 1G). This represents a feature for V4 direction-preferring domains that we have not observed in other areas. Our qualitative inspection gives the impression that direction-preferring domains overlap with both color- and orientation-preferring bands in V4, something that we quantify later.

The small size of the direction-preferring domains in V4 raises the possibility that they emerge randomly due to noise. To examine this possibility, we generated a "random map" using the same data from Figure 1H by randomly swapping, in half of the trials, the values in the t test comparison. The resulting random map (Figure 1I) was processed in an identical way to that of the map in Figure 1H and reveals a flat gray map that lacks any visually significant domains. This provides support that the domains we observed in the V4 direction preference map are not artifacts and are indeed related to the direction of stimulus motion. In addition, the time courses of the responses within the direction-preferring domains show that a direction preference emerges approximately 0.5–1 s after the stimulus onset and is maintained throughout the stimulus session (see Figure S3).

Figures 1G and 1H show the global aspects of direction-preferring domains in V4. Figure 2 presents details for the three direction-preferring regions in V2 (Figures 2A and 2D) and V4 (Figures 2B, 2C, 2E, and 2F). As in Figures 1G and 1H, each panel in Figures 2A–2C is a paired t test comparison between two opposite-direction stimuli. Direction preference maps for all eight directions are presented for each region in the same spatial scale. Figures 2D–2F represent the vectorized summation of the corresponding direction preference maps on the left (i.e., polar maps). Both the V2 and V4 direction preference maps contain different domains that respond to each of the eight directions. We found that the direction-preferring domains in V4 (average diameter, 361 ± 13 μm, n = 44) are slightly larger than those in V2 (321 ± 12 μm, n = 35; two-tailed t test, $p = 0.03$). In both V2 and V4, direction-preferring domains are significantly smaller in size than are orientation-preferring domains (V4, 542 ± 17 μm, n = 73; V2, 556 ± 20 μm, n = 78) or color-preferring domains (V4, 527 ± 32 μm, n = 25; V2, 470 ± 26 μm, n = 24). Size comparisons between V2 and V4 for the same type of domains (orientation- or color-preferring domains) reveal no significant differences (two-tailed t test, $p > 0.05$). Instead of size, the direction-preferring domains in V2 and V4 appear to differ in how their domains are organized. While V2 domains preferring different directions are always tightly clustered, V4 direction-preferring domains appear to be less regular and are scattered in a larger region. Many V4 domains appear to be isolated with no neighboring domains responding to other directions. Yellow circles in Figure 2B indicate one such domain. Within this ~1.5 mm region, only one domain (<0.5 mm) prefers the downward direction, but its neighboring regions do not have a directional

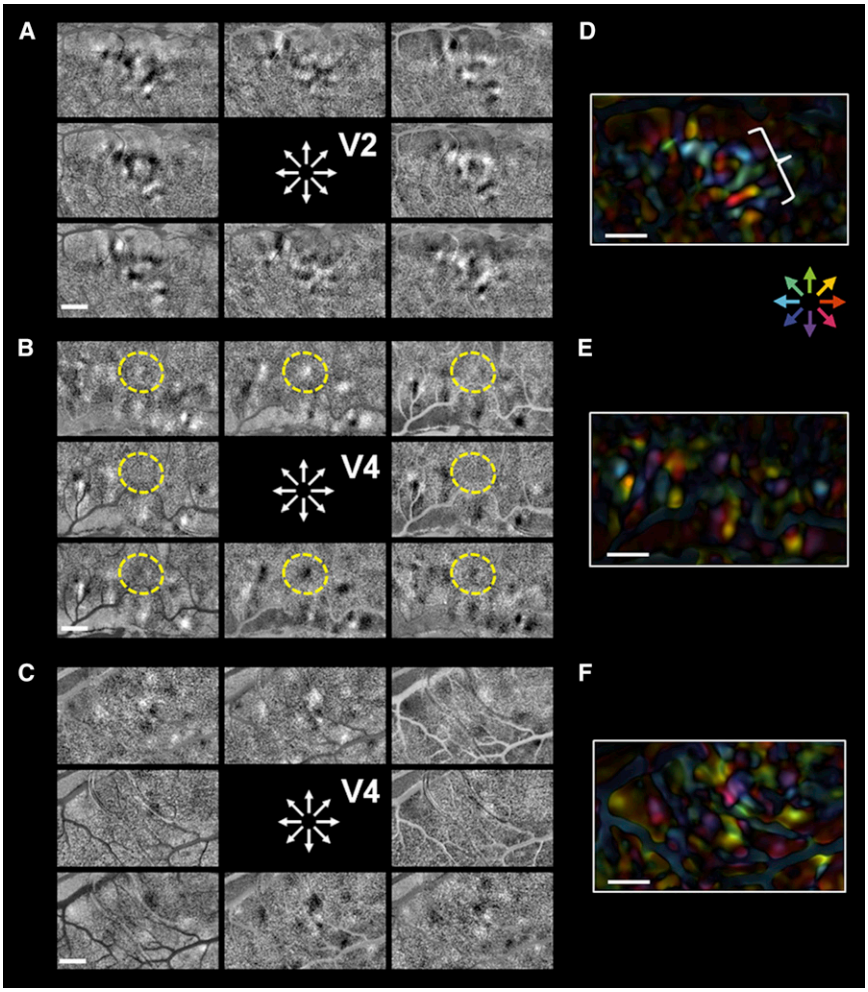

Figure 2. Close-Up Views of Direction-Preferring Domains in V2 and V4

(A–C) Responses from three direction-preferring regions to eight different directions in Case 1. (A) shows a V2 direction-preferring region (yellow arrowhead in Figures 1G and 1H); (B) and (C) show two V4 direction-preferring regions (bottom left and top left ovals in Figures 1G and 1H). Each small panel is the difference between the direction indicated by the corresponding arrow and its opposite direction. Yellow circles in (B) mark a singular downward-preferring domain in V4, which does not have any neighboring domains. This type of singular domain is often observed in V4 but not so common in V2.

(D–F) Vectorized summations of the eight small panels in (A) through (C). Each direction is coded in a specific color; the color index is shown under (D). Note that, in (A), locations of the V2 activation zones shift as stimulus direction shifts, forming a linear shifting region, indicated with a white bracket in (D). In contrast, direction-preferring domains in V4, shown in (B) and (C), often appear as isolated singular domains. Their polar maps, shown in (E) and (F), also have few linear patterns; nevertheless, representation for every direction (every color) can be found in these direction preference maps. Scale bars, 1 mm.

preference (mostly gray pixels within the yellow circles). Although only a minority of V4 direction-preferring domains exhibit such a "singular" form, this may represent a new feature in functional maps. In some V4 direction preference maps, certain direction-preferring domains may have stronger activation than others. In Figure 2C, we show domains with a stronger response to the up and down directions but weaker overall left or right direction-preferring domains. These features result in fewer pinwheels or linear patterns in the V4 direction polar maps (Figures 2E and 2F), while these features are more common in V2 (white bracket in Figure 2D; also see Lu et al., 2010). When pixel numbers are quantified, the direction-preferring domains only cover approximately 3.4% of the total V4 area, in comparison with 8.9% coverage for color-preferring domains and 24.6% for orientation-preferring domains. Our quantification in V2 shows that the coverage of direction-, color-, and orientation-preferring domains are 6.6%, 12.7%, and 53.2%, respectively.

In the present study, we observed direction preference maps in seven out of eight hemispheres examined. One case lacked obvious direction preference maps, due to an overall weak signal in that imaging experiment. Figure 3 illustrates three cases (Case 2–4) in which the V4 was imaged. The location of imaging windows (illustrated in the top left corner) is similar to that in Case 1 but in the left hemisphere. Determination of V1, V2, and V4 was based on the same criteria as in Case 1, and all maps were obtained using the same stimuli. In Figure 3, each case is presented in one row. Ocular dominance maps (first column), color preference maps (second column), orientation preference maps (third column), and direction preference maps (fourth column) are presented for each case. Generally, these maps have similar features to those observed in Case 1. We observed ocular dominance, orientation preference, and color preference maps in V1 that are consistent with prior studies (Lu and Roe, 2008). We found that the exposed size of V2 was more constant in anteroposterior extent (~2 mm) in some cases (Cases 2 and 3) and became broader laterally in others (Cases 1 and 4). These three cases exhibit a more obvious stripe structure in V2 than in Case 1; all exhibit an interdigitating orientation and color organization (red lines indicating V2 color-preferring response regions). In V4, similar to Case 1, orientation- and color-preferring domains appear to dominate the complementary regions of V4. In some locations, a banding structure can be seen, although there appears to be significant variability across cases. Of note, we find that direction-preferring domains exist in V4 in nearly all cases. These domains are small and, like orientation- and color-preferring domains, appear only in restricted regions of V4 (yellow circles). V2 direction-preferring domains are also visible in these direction preference maps, although the stimulus used here (square-wave gratings) is not as effective as random

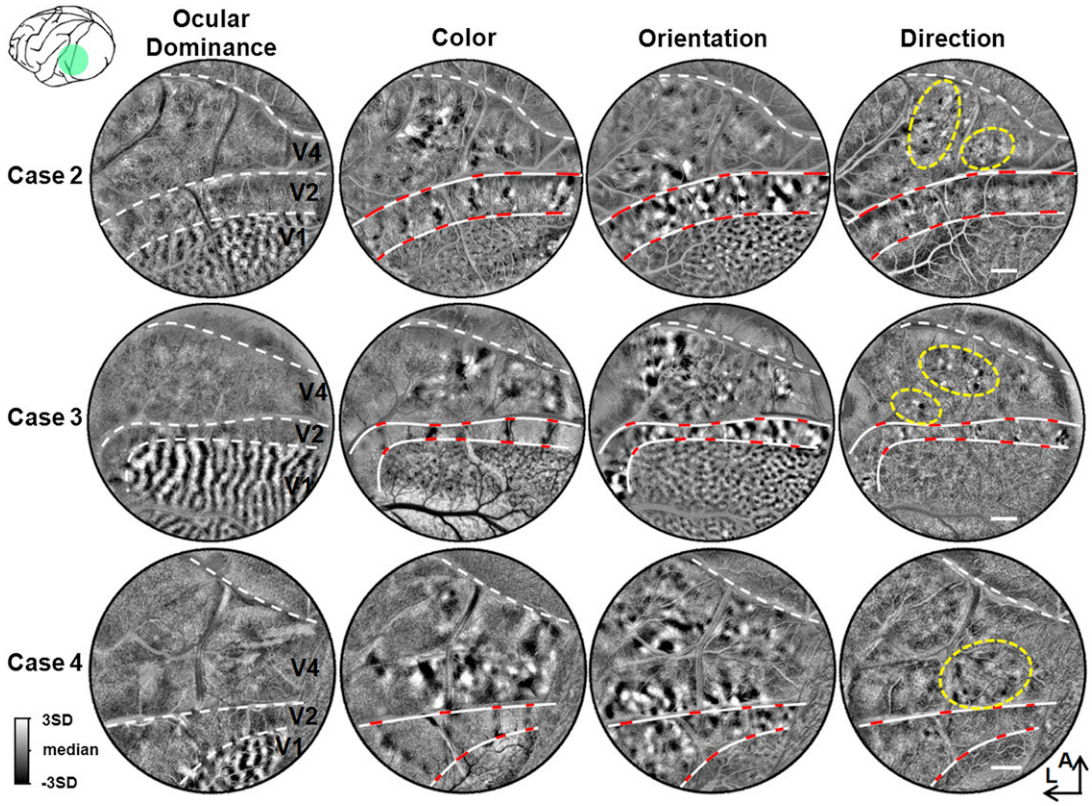

Figure 3. Functional Maps from Cases 2–4

One case is shown per row. All three cases are taken from the left hemisphere (illustrated in inset at top left corner). The four columns are as follows: ocular dominance maps (first column), color preference maps (second column), orientation preference maps (third column), and direction preference maps (fourth column). Maps were obtained using the same stimuli as those used in Case 1. Generally, these maps have similar features to those observed in Case 1. In V4, patches of color-, orientation- and direction-preferring domains appear to occupy restricted regions. From case to case, a large variation of V4 domain locations was observed, unlike a uniform distribution in V1 or a periodical distribution in V2. Nevertheless, direction-preferring domains were observed in V4 in every case. Plot conventions are the same as in Figure 1. A, anterior; L, lateral. Scale bars, 2 mm; different cases (rows) show different scale bars.

dots in revealing these domains (cf. Lu et al., 2010). In general, unlike V1 and V2, the locations of V4 orientation-, color-, and direction-preferring domains do not exhibit consistent patterns across cases.

Direction preference maps can be repeatedly imaged from the same locations on different days when a chronic chamber was implanted. Figure 4 presents a case (Case 8) in which three imaging experiments were performed using the same experimental protocols. Images in the three rows are obtained from three different experiments that are at least 1 week apart. From left to right, the images in each column are chamber photos, surface blood vessel patterns, orientation preference maps, direction preference maps, and close-up views of V4 direction preference maps. Despite some small changes in blood vessel patterns and noise levels, the overall orientation preference and direction preference patterns are the same across different days. This indicates that the V4 direction preference map, like the V4 orientation preference map, is an intrinsic and stable feature of this area.

Direction preference maps in V4 can be obtained from a wide range of stimulus parameters (e.g., sine- or square-wave gratings; spatial frequency [SF] range = 0.3–2.4 cycles per degree [c/deg]; temporal frequency [TF] range = 1–8 Hz). The optimal activation is seen with square-wave gratings at a periodicity of 1.5 c/deg (0.13° white and 0.53° black each cycle) and speed of 5.33°/s (direction preference maps in Figures 1 and 3). In all the cases, V4 direction-preferring domains have some overlap with the color-preferring domains; thus, we considered the possibility that direction activation may be caused by subtle color differences in oppositely moving gratings (e.g., due to chromatic aberration). To rule out this possibility, we created narrow-band wavelength gratings by placing color filters in front of the monkeys' eyes. Two types of filters were used (546 nm or 630 nm, bandwidth 20–30 nm; these were the same filters we used for illumination in optical imaging). The direction stimuli presented on the screen were the same as those we used in all other experiments. Through these filters, the monkey viewed either green-black (for 546-nm filter) or red-black (for 630-nm filter) gratings. For such a narrow bandwidth light, the chromatic aberration is negligible. We obtained V4 direction-preferring domains in which the domain patterns are the same as those obtained with the black/white luminance gratings (Figure S4A). Note that the common color activation was subtracted out so these maps do not reflect color activation. Similarly,

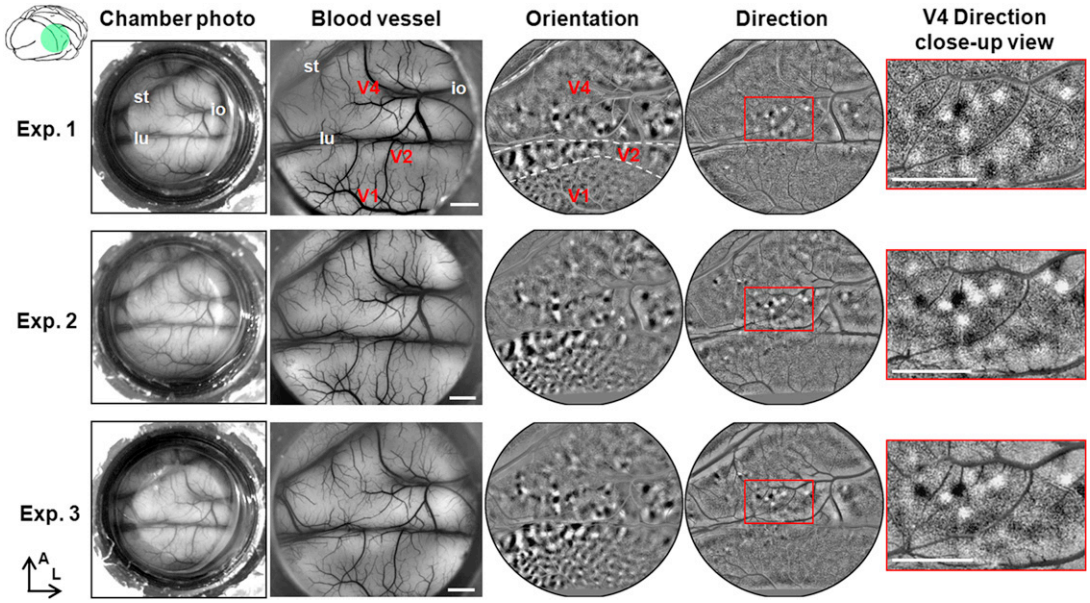

Figure 4. Chamber Photos and Functional Maps of the Same Cortical Region across Several Days

Images in the three rows were collected on three different days. The first column shows photos of the imaging chamber taken by a digital camera, and the second column shows blood vessel images obtained with the imaging camera under 546 nm green light illumination; their labels in the first row indicate major sulci (lu, lunate; st, superior temporal; io, inferior occipital sulcus) and visual areas (V1, V2, and V4). The third column shows orientation preference maps (horizontal versus vertical gratings). Dotted lines indicate area boundaries between V1, V2, and V4. The fourth column shows direction preference maps (upward versus downward directions), from which the framed regions are expanded in the fifth column. These maps show that V4 direction-preferring domains, like orientation-preferring domains, can be repeatedly imaged from the same locations on different days. Functional maps from different days were aligned based on blood vessel maps. Scale bars in the second and fifth columns, 2 mm.

See Figure S4.

orientation preference maps obtained with these color gratings are the same as those from luminance gratings. Since narrowband filters only permit one color to pass through, this excludes the possibility that the direction preference map is due to different colors in two oppositely moving directions.

We also considered the possibility that some of the observed responses could be due to phase differences between gratings presented to the two eyes. In most cases, we did not align the two eyes so such phase difference could arise because each eye was looking at different areas of the full-screen gratings. Any single drift direction could be associated with a different interocular phase disparity than that in the opposite drifting direction. Interocular phase difference could activate disparity neurons in the visual cortex (Anzai et al., 1997). To examine whether the direction preference maps we observed are related to binocular disparity, we performed the same imaging procedures with one eye covered. With these experiments, we found that monocular stimulation produced very similar direction preference maps (Figure S4B). In addition, in several cases, we also imaged V4 direction preference maps with gratings containing multiple spatial frequencies (i.e., one-dimensional noise patterns). Such gratings have variable interocular phases and should not cause systematic bias between different conditions. These resulted in the same direction preference maps in V4 (data not shown). We conclude that the direction preference maps we observed in area V4 are not due to binocular disparity in the visual stimulus.

Single-Cell Recordings Support Optical Imaging Results

To study the neuronal response underlying these direction preference maps in V4, we performed single-cell recording from three macaques under anesthesia. Recordings were made that targeted regions either at the center of a direction-preferring domain or regions away from direction-preferring domains, based on direction preference maps and surface blood vessel maps imaged on the same day. Figures 5A–5C shows one case in which recordings were made from three direction-preferring domains and one location away from direction-preferring domains. Figure 5A shows a direction polar map in which different colors represent different directions that provides an overall view of the direction selectivity of the region. In selecting a recording location, the two-condition direction preference maps (e.g., Figures 1G and 1H) were also checked to make sure the recordings were made from the center of, or away from, a direction-preferring domain. In the example illustrated in Figure 5A, the locations of four recording sites (white crosses) are marked on the polar map as well as on the blood vessel map imaged on the same day (Figure 5B). The response of a cell to gratings drifting in one of eight directions inside its classical receptive field was measured. The isolation of single cells was confirmed for each cell based on the cell's spike waveforms and interspike intervals (see Figure S5). All cells recorded were confirmed to be single cells. Figure 5C shows direction tuning polar plots for 19 cells recorded from the four penetrations (four rows) at different depths (labeled on the top of the polar

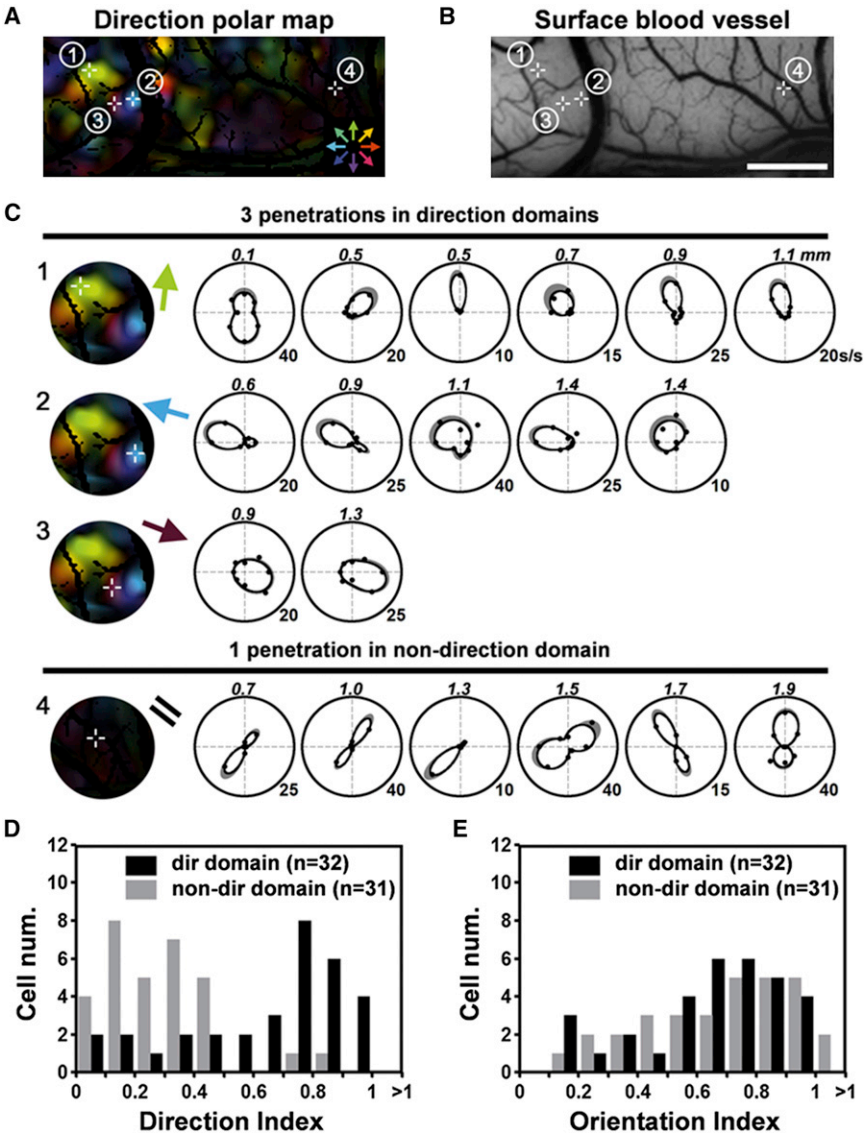

Figure 5. Clustering of Direction-Selective Neurons in V4 Direction-Preferring Domains

(A) Color-coded direction polar map illustrates the locations of four recoding sites (sites 1–3: direction-preferring domains, site 4: non-direction-preferring domain).

(B) Blood vessel image of the same cortical region used to guide electrode penetrations. Scale bar, 1 mm; this also applies to (A).

(C) Direction selectivity of 19 neurons recorded from four penetrations. The imaged polar maps on the left indicate the direction selectivity (sites 1–3, colored arrows) or the orientation selectivity (site 4, bars) at the recording site. Direction polar plots on the right show the direction selectivity of single neurons recorded from the same penetration at different depths (see label at top of each plot). In each polar plot, response spike rates (black dots) are fitted with a von Mises function (black curve), and the gray region around the tuning function represents 1 SEM. Most neurons recorded in direction-preferring domains showed strong direction selectivity, and their preferred direction was consistent with the optical imaging results. Neurons recorded from non-direction-preferring domains showed weak or no direction selectivity.

(D) Distributions of direction selectivity index values (DI = 1 − Rn/Rp) for all neurons collected in direction-preferring domains (black bars) and in non-direction-preferring domains (gray bars). Neurons in direction-preferring domains showed much higher direction selectivity than those in non-direction-preferring domains ($p = 1.01 \times 10^{-6}$, Kolmogorov-Smirnov test).

(E) Distribution of orientation selectivity index values for the same neurons collected in direction-preferring domains (black bars) and in non-direction-preferring domains (gray bars). These two groups of neurons do not differ in orientation selectivity ($p = 0.48$, Kolmogorov-Smirnov test).

See Figure S5.

plots). The depth is measured based on the readout of the microdrive after a visual assessment of cortex surface. Optical imaging polar maps (magnified from Figure 5A) and the corresponding direction preferences (colored arrows) are shown on the left. Most cells recorded from direction-preferring domains exhibit directional selectivity, while those recorded outside direction-preferring domains are mainly not directional selective. For example, five out of six cells in penetration 1 show strong direction selectivity. The preferred directions of these five direction cells (95.3° ± 13.4°) are close to the direction preference of the recording site revealed from optical imaging (82.9°; green arrow in Figure 5C). This indicates a columnar organization of direction-selective neurons in direction-preferring domains. There is also a certain degree of heterogeneity in the direction-preferring domains. For example, one cell did not show significant direction selectivity (cell 1, Direction Index [DI] = 0.33), while others are strongly (cell 3, DI = 0.99) or weakly (e.g., cell 5, DI = 0.71) directional. In non-direction-preferring domains, we also recorded a few direction-selective cells (e.g., cell 3 in penetration 4). However, direction-selective neurons were very rare in regions outside of the direction-preferring domains. In three cases, we recorded 32 cells from seven direction-preferring domains. Twenty-three (72%) of these were direction selective ($p < 0.05$, Rayleigh test for circular uniformity). Another 31 cells were recorded from nine locations outside of direction-preferring domains. Only two out of these 31 cells (6.5%) were direction selective ($p < 0.05$, Rayleigh test; DIs = 0.71 and 0.85, respectively). The distributions of direction selectivity and orientation selectivity of cells inside (black) versus outside (gray) direction-preferring domains are plotted in Figures 5D and 5E, respectively. Cells recorded from inside direction-preferring domains (DI, 0.63 ± 0.05, n = 32) have higher direction selectivity than cells recorded outside direction-preferring domains (DI, 0.28 ± 0.03, n = 31; $p = 1.01 \times 10^{-6}$, two-sample Kolmogorov-Smirnov test

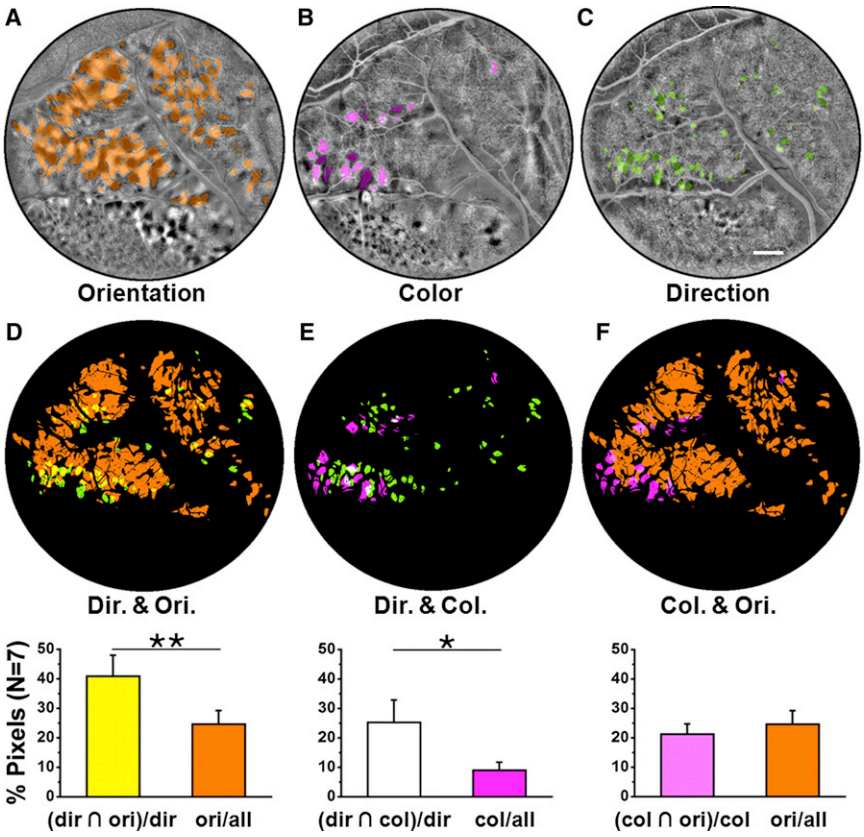

Figure 6. Overlap between V4 Functional Maps

(A–C) Orientation- (A), color- (B), and direction (C)-preferring maps from Case 1, same as Figures 1E, 1D, and 1G, respectively. Domain masks are overlaid on to the representative maps with different colors (orange, orientation mask; pink, color mask; green, direction mask). Scale bar, 2 mm; this applies to (A) through (F).

(D) Top shows spatial overlaps between direction (green) and orientation (orange) maps revealing significant overlapping pixels (yellow). Bottom shows the percentage of direction pixels overlapping with the orientation mask (yellow bar) is significantly larger than the percentage of orientation pixels in total V4 areas (orange bar) ($p = 0.002$, two-tailed t test, $n = 7$), which indicates a tendency of direction and orientation preference maps to overlap.

(E) Similarly to (D), comparison of direction and color masks also indicates a tendency for direction and color preference maps to overlap in V4 ($p = 0.023$, two-tailed t test, $n = 7$).

(F) Color and orientation do not show a tendency to overlap ($p = 0.20$, two-tailed t test, $n = 7$). Error bar, 1 SEM.

See Figure S6.

for equal distributions). In contrast, the orientation selectivity of these two groups of neurons is not significantly different ($p = 0.48$, two-sample Kolmogorov-Smirnov test). These observations indicate that V4 directional neurons are concentrated in direction-preferring domains and provide further support for the directional nature of these domains.

Spatial Relationship with Orientation/Color Preference Maps

In V2, direction-preferring domains tend to overlap with orientation-preferring domains but avoid color-preferring domains (Lu et al., 2010). In V4, orientation and color preference maps tend to segregate spatially (Tanigawa et al., 2010). This spatial segregation has been interpreted to indicate some degree of functional independence, while spatial overlap suggests a greater degree of modal integration. Here, we quantitatively evaluated the spatial relationship between direction-preferring domains and orientation- and color-preferring domains. Figures 6A–6C show orientation (Figure 6A), color (Figure 6B) and direction (Figure 6C) preference maps from Case 1 (same as in Figures 1E, 1D, and 1G, respectively). Each map is overlaid with corresponding domain masks to show general correspondence (orange for orientation mask, pink for color mask, green for direction mask). Domain masks were calculated from p-maps at a fixed threshold level (see Experimental Procedures). Pixels from blood vessels were removed from these masks. These masks were then overlaid in pairs in Figures 6D–6F.

In Figure 6D, V4 direction-preferring domains (green) have some overlap with orientation-preferring domains (orange). We calculated the percentage of pixels in these overlapped regions in the total direction-preferring domains. We reasoned that, within a region, if the direction-preferring domains and orientation-preferring domains are truly independent (i.e., the direction-preferring domains have no particular spatial relationship with the orientation-preferring domains), the percentage of direction-preferring domain pixels overlapping with orientation-preferring domains would be at the chance level (i.e., would not be different from the percentage of orientation pixels in the whole V4 area). If direction-preferring domains contain more orientation-selective pixels than the V4 average, then this would indicate an overlapping that is greater than chance between these two types of domains. Figure 6D shows that the percentage of orientation pixels in the direction-preferring domains is higher than the percentage of orientation pixels in V4. Averaging across all seven cases, 40.8% ± 7.1% of the pixels in the direction-preferring domains have a significant orientation response, compared to 24.6% ± 4.7% of all V4 pixels (two-tailed t test, $p = 0.002$). This difference demonstrates a tendency for direction- and orientation-preferring domains to overlap. Furthermore, for pixels within the orientation-direction overlap regions, their preferred direction is always orthogonal to their preferred orientation (Figure S6), a common functional property for direction-preferring domains in different areas and different species (Malonek et al., 1994; Weliky et al., 1996; Shmuel and Grinvald, 1996; Lu et al., 2010). Similar to the direction-orientation overlap, Figure 6E shows that more pixels in direction-preferring domains (25.3% ± 7.6%) have a significant color

response than the proportion of color response pixels in the whole V4 area (8.9% ± 2.7%, two-tailed t test, p = 0.023). In contrast, Figure 6F shows that, although areas that show orientation preference and color preference have some overlap, the degree of their overlap does not exceed a chance level (two-tailed t test, p = 0.2).

DISCUSSION

To examine the representation of directional response in the macaque ventral visual pathway, we imaged large fields of view over the foveal and parafoveal regions of V4 and adjacent regions of V1 and V2. No previous study has simultaneously examined such a large extent of all three regions in the macaque monkey (cf. Ghose and Ts'o, 1997; Tanigawa et al., 2010). Consistent with previous findings (Lu et al., 2010), we found a lack of functional organization for directional response in V1 and the presence of directional domains in V2 thick/pale stripes. In V4, we found that domains of directional preference were distributed in restricted regions. Single-cell recordings targeting these direction-preferring domains confirmed the columnar organization of direction-selective neurons in these domains. Some direction-preferring domains in V4 also overlapped with both color- and orientation-preferring domains in V4.

V4 Direction Preference Map

Unlike previously reported motion maps, the V4 motion map we report here is in the ventral pathway. We demonstrate that such a map exists in nearly all the monkeys we examined. The same direction-preferring domains could be repeatedly imaged from the same regions on different days or using different stimulus paradigms. Although V4 directly borders V3, a motion-sensitive area located between V2 and V4, it is unlikely that the direction-preferring domains we observed are from V3. First of all, previous studies have shown that area V3 is buried in the lunate and inferior occipital sulci (e.g., Gattass et al., 1988; Felleman and Van Essen, 1987, Figure 3; Stepniewska et al., 2005). In addition, the direction-preferring domains we observed are not particularly close to the lunate sulcus, as would be expected if part of V3 was exposed on the surface (between lunate sulcus and area V4).

The fact that V4 direction-selective neurons systematically cluster within small regions has meaning beyond simply the presence of direction signals in the area. A map itself may not be functional (Horton and Adams 2005); however, clustered neurons have greater chances to form efficient connections, which is typically indicative of an active computational process within that particular region (Chklovskii and Koulakov 2004). Maps of common features have been demonstrated in many visual areas: for example, orientation and color preference maps in V1, V2, and V4; direction preference maps in MT; and color preference in posterior inferior temporal cortex (Conway and Tsao 2009). The existence of a direction preference map in V4 suggests that V4 not only has access to motion information (through feed-forward inputs and/or from dorsal areas) but also actively processes this information for certain purposes, which may be critical for the function of this area. The finding of a direction preference map in V4 also provides a venue for further study of these functional and anatomical properties of V4 direction-selective neurons with, for example, map-guided tracer injection or electrophysiological recording, which were very difficult without a map.

Direction preference maps have been found in the primary visual cortex of cats (Shmuel and Grinvald, 1996) and ferrets (Weliky et al., 1996), in area MT of owl monkeys (Malonek et al., 1994; Kaskan et al., 2010) and bush babies (Xu et al., 2004), and in the thick/pale stripes of macaque V2 (Lu et al., 2010). The direction preference map in V4 showed some common properties as those found in MT and V2, including similarity in domain size and the orthogonal relationship between preferred direction and orientation angles (Lu et al., 2010; Kaskan et al., 2010). However, the direction preference maps in V4 also showed features that are distinct from those found in all these other areas. First, V4 direction-preferring domains only appear in restricted regions, rather than in the entire V4 area. Second, many V4 direction-preferring domains appear to be isolated singulars, without any neighboring domains for other directions. Third, these domains overlap not only with orientation-preferring domains but also with color-preferring domains. It is understandable that a direction map in the ventral pathway may have a different clustering architecture than its counterparts in the dorsal pathway. A precedent for this principle was found, for example, in motion maps of V2 (Lu et al., 2010), where the direction maps differ in architecture from those found in MT (Malonek et al., 1994; Xu et al., 2004; Kaskan et al., 2010) or cat area 18 (Shmuel and Grinvald, 1996). Thus, this functional architecture may suggest a distinct functional computation in the visual system.

Direction-preferring domains found in previous studies either have been shown in an area not considered to signal color (e.g., MT; Malonek et al., 1994; Xu et al., 2004; Kaskan et al., 2010) or avoid color-preferring regions (e.g., in thick/pale stripes of V2; Lu et al., 2010). Our data show that, in V4, about one fourth of direction-preferring pixels overlap with color-preferring pixels, suggests that these direction-selective neurons may be involved in detection of color motion. Another possibility is that motion cues in V4 are used for surface definition and thus are processed by surface-processing neurons, which were revealed by color versus luminance imaging (e.g., Figure 1D). These results, however, differ from the findings in a recent fMRI-guided recording study in which color cells recorded from globs rarely showed direction selectivity (Conway et al., 2007). We noted that the V4 color glob neurons they recorded from were mostly from anterior wall of the lunate sulcus, while our imaging and recordings were all from dorsal part of the lunate gyrus. Therefore, it is possible that different parts of V4 may have different color-direction interactions.

Parallel Processing of Motion and Color/Form Information?

The separation of motion and color/form information in the primate visual system has been considered to be strong support for the concept of parallel processing of visual information. In particular, areas MT and V4 are often referred to as motion and color/form centers, respectively (Zeki et al., 1991). However, accumulating evidence has shown that the same type of

information does exist in both pathways and that visual areas belonging to different pathways often interact with each other (see review of Nassi and Callaway, 2009). Evidence from human patient studies suggests that the functional differences of the dorsal and ventral pathways are better explained by vision-for-action and vision-for-perception, respectively (Goodale and Milner, 1992). In fact, V4 receives mixed magnocellular and parvocellular inputs originating from the lateral geniculate nucleus (Ferrera et al., 1994a), as well as input from MT (Maunsell and Van Essen, 1983; Ungerleider and Desimone, 1986). These connections make V4 an area that has rich access to motion information in the visual stimulus. Furthermore, it has been shown that top-down signals to V4 also contain motion information (Ferrera et al., 1994b). As a result, V4 is well activated when monkeys are viewing moving stimuli (Tolias et al., 2001; Vanduffel et al., 2001). Our findings further suggest that the motion information is actively processed in this area. Note that V4 is much larger than MT, so V4 may contain a comparable number of direction-selective neurons as area MT. This may raise the question, "Why would both dorsal and ventral pathways participate in motion processing?" A reasonable assumption is that the same motion information needs to be processed in different ways in order to serve different purposes. For example, motion perception requires integration of local motions, while distinguishing a moving object from its background requires motion differentiation (Braddick 1993). We found that the motion-processing organization in V4 is different from that in MT. For example, many direction-preferring domains in V4 are scattered singulars, while direction preference maps in MT are more uniform (Malonek et al., 1994; Xu et al., 2004; Kaskan et al., 2010). The mean direction selectivity of neurons recorded in the V4 direction-preferring domains (mean DI = 0.63; this study) is lower than that found in area MT (mean DI = ~1; Albright et al., 1984). V4 neurons also tend to be more activated by moving lines than by moving random dots (Baker et al., 1981; Vanduffel et al., 2001). In addition, motion adaptation could induce direction selectivity of V4 neurons (Tolias et al., 2005). These data suggest that the direction-selective neurons in V4 have very different receptive field features than do MT neurons. These differences could give us hints on the functional roles of direction-selective neurons in the ventral pathway. It is also possible that perception of motion might be a distributed process that is not limited to the dorsal areas. This idea is supported by a recent finding that MT does not process global motion (Hedges et al., 2011).

Form-from-Motion Processing in the Ventral Pathway

Motion information is useful for object identification. Relative motion between an object and its background is an important cue for figure-ground segregation, especially when other types of cues are weak or ambiguous (e.g., camouflaged insects). Orban and his colleagues have studied neurons in multiple visual areas (V1, V2, V4, MT, and IT) using kinetic boundary stimuli (Sáry et al., 1993, 1995; Marcar et al., 1995, 2000; Mysore et al., 2006, 2008). Kinetic boundaries were generated by stripes of random dots moving in opposite directions. It is interesting that they found that the majority of V4 neurons respond significantly to random dot stimuli that contain kinetic boundaries, more so than to random dots having uniform motion or transparent motion. A considerable proportion of these neurons (10%–20%) also have the same orientation preference for the kinetic and luminance boundaries (Mysore et al., 2006). This is significantly different from what occurs in area MT, in which virtually no neuron displayed orientation selectivity for such kinetic boundaries (Marcar et al., 1995). By analyzing electrode penetration locations in V4, Mysore et al. (2006) also found that these kinetic-boundary-selective neurons tend to cluster in small regions of V4. V4 neurons are also selective to shapes defined by motion (Vanduffel et al., 2002; Mysore et al., 2008; Handa et al., 2010). Most importantly, measurements of response latency to kinetic boundaries indicate that the kinetic boundary detection might be done locally in V4 (Mysore et al., 2006). Direction-selective neurons in V4 may therefore provide necessary motion information either directly to these kinetic boundary-selective neurons or through some intermediate neurons that perform local motion comparisons. The functional structure of direction-preferring domains in V4 therefore may play an important role in facilitating the computation of boundaries or shapes inferred from motion cues.

In summary, our data demonstrate the existence of motion maps in a ventral visual area. This finding suggests that motion-sensitive neurons in this area may contribute to form and/or motion processing. This finding also provides information contributing to a re-evaluation of dorsal/ventral separation as a general rule in visual information processing. A map of direction-selective neurons also facilities future studies of motion processing in V4. This information could contribute significantly to our understanding of area V4 and how motion is processed in the brain.

EXPERIMENTAL PROCEDURES

All procedures were performed in accordance with the National Institutes of Health Guidelines and were approved by the Institutional Animal Care and Use Committee, Institute of Neuroscience, Chinese Academy of Sciences. A total of eight hemispheres from eight macaque monkeys (seven *Macaca mulatta* and one *Macaca fascicularis*) were examined (these monkeys also participated in other studies).

Surgery

Monkeys were artificially ventilated and anesthetized with isoflurane (1%–2.5%) during surgery. A 25-mm-diameter circular craniotomy and durotomy were performed (center location, 28–38 mm from midline, 12–17 mm from posterior bone ridge) to expose visual areas V1, V2, and V4 (see Figure 1A). During imaging sessions, a paralytic drug (vecuronium bromide, 0.05 mg/kg/hr) was administered intravenously (i.v.) to prevent eye movement, and the anesthesia was switched to thiopental sodium (1–3 mg/kg/hr i.v.). Anesthetic depth was assessed continuously via monitoring the heart rate, end-tidal CO_2, blood oximetry, and, in some cases, electroencephalogram. Eyes were dilated (atropine sulfate) and fit with contact lenses of appropriate curvatures to focus on a screen 57 cm from the eyes.

Optical Imaging

Following craniotomy surgery, the brain was stabilized with agar, and images were obtained through a cover glass. Images of reflectance change (intrinsic hemodynamic signals) corresponding to local cortical activity were acquired (Imager 3001, Optical Imaging Inc., Germantown, NY) with 630 nm illumination (Lu and Roe, 2007). Signal-to-noise ratio was enhanced by trial averaging (30–50 trials per stimulus condition). Frame sizes were either 504 × 504 pixels or 540 × 654 pixels representing either 19 × 19 mm or 20 × 24 mm of imaged area. Visual stimuli were presented in blocks. Each block contained all

stimulus conditions (e.g., different orientation gratings) and a blank condition, which is a gray screen at the same mean luminance level as grating conditions. The same gray screen is used for interstimulus intervals (ISI), which were at least 8 s. For each condition, imaging started 0.5 s before the stimulus onset (imaging of the baseline) while the screen remained as a gray blank (the same as in the ISI). Then a visual stimulus was presented for 3.5 s. Therefore, the total imaging time for each condition is 4 s, during which 16 consecutive frames were imaged (i.e., 4 Hz frame rate). All stimulus conditions were displayed in a randomized order.

Visual Stimuli

Visual stimuli were created using ViSaGe (Cambridge Research Systems Ltd.) and presented on a 20-in. cathode ray tube monitor (SONY CPD-G520). The stimulus screen was gamma corrected and positioned 57 cm from the eyes. For ocular dominance, orientation, and direction preference maps, full-screen drifting square-wave gratings were used. Each cycle of the square-wave gratings is 0.67° wide (0.13° white, 0.53° black, equivalent to periodicity of 1.5 c/deg, and duty cycle of 0.2). The mean luminance for all stimuli, including the blank, was kept at 8 cd/m^2. Gratings were drifting at 5.33°/s (8 Hz) and were presented in a randomly interleaved fashion in one of eight directions (0°, 45°, 90°, 135°, 180°, 225°, 270°, or 315°). The initial phases of the gratings were also randomly selected. For color preference maps, responses to red-green isoluminant sinewave gratings and black-white sinewave gratings were compared. Gratings were presented in one of two orientations (45°, 135°) and random directions. Data from different orientations were pooled. In red-green gratings, red CIE (Commission Internationale de l'Eclairage [International Commission on Illumination]) values were 0.552 and 0.299; green CIE values were 0.268 and 0.530. In black-white gratings, the luminance was modulated at 100% contrast. These two types of gratings were set at the same SF (0.15 or 1 c/deg), TF (1 or 4 Hz) and mean luminance level (19 or 36 cd/m^2) so that the only difference between these two types of gratings were their color contents (Lu and Roe, 2008).

Imaging Data Analysis

For each stimulus condition, a percentage change map (dR/R) was first calculated using the following formula: dR/R = ($R_{8-16} - R_{1-4}$)/R_{1-4}, in which R_{1-4} is the average of frames 1–4 and R_{8-16} is the average of frames 8–16. Each dR/R map was filtered (digital Butterworth four-order filtering, low- and high-pass cutoff sizes: 34–38 μm per cycle and 1.02–1.52 mm per cycle). We used t-maps (Wang et al., 1996, Xiao et al., 2007) instead of subtraction maps to represent differential response to different stimulus features. For each pixel in a t-map, its t value is based on the pixel's response to two stimulus conditions. For any pixel i, its paired t value (t_i) is calculated as follows: $t_i = (\overline{C1}_i - \overline{C2}_i) * \sqrt{N}/S_i$ in which $\overline{C1}_i$ and $\overline{C2}_i$ are the means of pixel i's optical response (dR/R) to stimulus conditions 1 and 2. S_i is the SD of $(C1_i - C2_i)$, and $\sqrt{N}$ is the square root of the sample size (number of repeats). Thus, a t-map is similar to the classical subtraction map (i.e., $\overline{C1}_i - \overline{C2}_i$), except that each pixel is divided by its trial-to-trial variation value. A t-map takes into account the amount of variance, so pixels having large variance will have smaller t values. Figure S2 shows the comparison of t-maps and conventional subtraction maps calculated from the same data sets. Both maps reveal the same functional domains in V4. Nevertheless, the large amount of noise in blood vessel regions is better suppressed in the t-maps than that in the subtraction maps. Polar maps (vector summation of eight conditions) were also calculated for direction and orientation selectivity. To obtain a polar map, each dR/R map was first filtered (digital Butterworth four-order filtering, low- and high-pass cutoff sizes: 170–190 μm per cycle and 1.02–1.52 mm per cycle) and compared with the dR/R map from the gray-screen blank condition to obtain a t-map. The t-maps from different directions/orientations were then vector-summed to obtain a polar map (Bosking et al., 1997). Masks for each type of domain (orientation, color, direction) were obtained from two-tailed P-maps in paired t tests. In the P-maps, regions that consisted of pixels with $p < 0.001$ and peak $p < 0.00001$ were considered to be significant responsive regions and were included in the masks. Since, in our preparation, V4 contains around 100,000 pixels, Bonferroni correction is not practical (high risk of type II error; see Perneger 1998; Lazar, 2008). The choice of threshold P value was based on the overall similarity in sizes between the resulting domains and the domains in the original difference maps. Here, we used more stringent P levels as a correction for multiple comparisons. After this thresholding procedure, a few noise pixels (close to blood vessel or as a result of filtering) were then removed manually. Orientation and direction masks were finally combined from masks obtained from orthogonal conditions. Domain size was calculated by averaging each domain's long and short axes measured from the t-map using ImageJ (National Institutes of Health).

Single-Cell Recording

Classical single-cell extracellular recordings (Hubel and Wiesel, 1968) were performed in three hemispheres of three anesthetized macaques. A recording chamber and a silicon hat (Arieli et al., 2002) were implanted following the initial optical imaging session. Electrode penetrations were made at specific V4 regions (either at the center of a direction-preferring domain or at a region far away from direction-preferring domains) guided by the cortical blood vessel patterns. Tungsten microelectrodes (impedance 1–4 MΩ at 1 kHz, FHC) were lowered into the cortex using a hydraulic microdrive (MO-97A, Narishige). Neural activity was amplified at 10 kHz (Model 1800, A-M Systems) and digitized at a sampling rate of 20 kHz (Power 1401, CED). Single-cell activity was isolated and sorted online (Spike2, CED). Once a single cell was isolated, its classical receptive field was plotted using a manually controlled bar and/or grating stimulus. Sine-wave or square-wave gratings drifting in eight different directions were then displayed within the cell's receptive field to measure orientation and direction preferences. The spatial and temporal frequencies of the gratings were adjusted to best drive the cell. Each stimulus presentation lasted 1 s and was followed by a 1 s ISI. In some experiments, we also used a 0.5 s stimulus presentation with a 1.5 s ISI. Usually, 10–25 repeats were collected for each stimulus condition.

Single-Cell Data Analysis

Neuronal responses to each direction were calculated by averaging the spike numbers during the stimulus presentation, shifted by a delay of 100 ms. The tuning functions were then fitted with a modified von Mises curve (Mardia, 1972) which fits well with both unimodal and bimodal distributions: $y = a + b1 * e^{c1*\cos(x-d1)} + b2 * e^{c2*\cos(x-d2)}$, in which x is the direction tested; y is the corresponding firing rate and is a function of x; a is the baseline offset; and (b1, b2), (c1, c2), and (d1, d2) determine the amplitude, shape, and position of the tuning curve, respectively. Fitting parameters were obtained with a least-square nonlinear regression method (nlinfit in Matlab, Mathworks). Goodness of fit (R^2) values were >0.7 for all units (n = 63) and were >0.9 for 52 out of 63 units.

Each neuron's direction-of-motion selectivity was determined using a DI based on a fitted response profile: DI = 1 − Rn/ Rp, in which Rp is the response to the preferred direction (direction that generated the maximum response) and Rn is the response to the null direction (direction that opposite to the preferred direction). DI values range from 0 to 1, with 1 being the maximum directional selectivity. Similarly, the orientation index (OI) was calculated as OI = 1 − Rn/ Rp, in which Rp is the response to a preferred orientation and Rn is the response to the orientation orthogonal to the preferred orientation. Gratings moving at two opposite directions were first averaged to obtain the orientation response. The Rayleigh test (Fisher, 1993) was used to test the significance of a neuron's direction selectivity. The Rayleigh test compares the circular data against a uniform distribution, where a rejection to the null hypothesis indicated a significantly deviation from uniformity. Neurons with $p < 0.05$ in the Rayleigh test were considered to be direction selective.

SUPPLEMENTAL INFORMATION

Supplemental Information includes six figures and can be found with this article online at http://dx.doi.org/10.1016/j.neuron.2013.02.024.

ACKNOWLEDGMENTS

We thank Dr. Anna W. Roe for valuable comments. We also thank Jingwei Pan, Junjie Cai, Cheng Xu, Zhongchao Tan, and Jie Lu for technical assistance. This

work was supported by grants from National Basic Research Program in China (973 Program 2011CBA00400); and the Hundred Talent Program of the Chinese Academy of Sciences.

Accepted: February 25, 2013
Published: April 24, 2013

REFERENCES

Albright, T.D., Desimone, R., and Gross, C.G. (1984). Columnar organization of directionally selective cells in visual area MT of the macaque. J. Neurophysiol. *51*, 16–31.

Anzai, A., Ohzawa, I., and Freeman, R.D. (1997). Neural mechanisms underlying binocular fusion and stereopsis: position vs. phase. Proc. Natl. Acad. Sci. USA *94*, 5438–5443.

Arieli, A., Grinvald, A., and Slovin, H. (2002). Dural substitute for long-term imaging of cortical activity in behaving monkeys and its clinical implications. J. Neurosci. Methods *114*, 119–133.

Baker, J.F., Petersen, S.E., Newsome, W.T., and Allman, J.M. (1981). Visual response properties of neurons in four extrastriate visual areas of the owl monkey (Aotus trivirgatus): a quantitative comparison of medial, dorsomedial, dorsolateral, and middle temporal areas. J. Neurophysiol. *45*, 397–416.

Bosking, W.H., Zhang, Y., Schofield, B., and Fitzpatrick, D. (1997). Orientation selectivity and the arrangement of horizontal connections in tree shrew striate cortex. J. Neurosci. *17*, 2112–2127.

Braddick, O. (1993). Segmentation versus integration in visual motion processing. Trends Neurosci. *16*, 263–268.

Conway, B.R., and Tsao, D.Y. (2009). Color-tuned neurons are spatially clustered according to color preference within alert macaque posterior inferior temporal cortex. Proc. Natl. Acad. Sci. USA *106*, 18034–18039.

Conway, B.R., Moeller, S., and Tsao, D.Y. (2007). Specialized color modules in macaque extrastriate cortex. Neuron *56*, 560–573.

Chklovskii, D.B., and Koulakov, A.A. (2004). Maps in the brain: what can we learn from them? Annu. Rev. Neurosci. *27*, 369–392.

Desimone, R., and Schein, S.J. (1987). Visual properties of neurons in area V4 of the macaque: sensitivity to stimulus form. J. Neurophysiol. *57*, 835–868.

Felleman, D.J., and Van Essen, D.C. (1987). Receptive field properties of neurons in area V3 of macaque monkey extrastriate cortex. J. Neurophysiol. *57*, 889–920.

Felleman, D.J., and Van Essen, D.C. (1991). Distributed hierarchical processing in the primate cerebral cortex. Cereb. Cortex *1*, 1–47.

Ferrera, V.P., and Maunsell, J.H. (2005). Motion processing in macaque V4. Nat. Neurosci. *8*, 1125, author reply 1125.

Ferrera, V.P., Nealey, T.A., and Maunsell, J.H. (1994a). Responses in macaque visual area V4 following inactivation of the parvocellular and magnocellular LGN pathways. J. Neurosci. *14*, 2080–2088.

Ferrera, V.P., Rudolph, K.K., and Maunsell, J.H. (1994b). Responses of neurons in the parietal and temporal visual pathways during a motion task. J. Neurosci. *14*, 6171–6186.

Fisher, N.I. (1993). Statistical Analysis of Circular Data (Cambridge, UK: Cambridge University Press).

Goodale, M.A., and Milner, A.D. (1992). Separate visual pathways for perception and action. Trends Neurosci. *15*, 20–25.

Gattass, R., Sousa, A.P., and Gross, C.G. (1988). Visuotopic organization and extent of V3 and V4 of the macaque. J. Neurosci. *8*, 1831–1845.

Ghose, G.M., and Ts'o, D.Y. (1997). Form processing modules in primate area V4. J. Neurophysiol. *77*, 2191–2196.

Handa, T., Inoue, M., and Mikami, A. (2010). Neuronal activity during discrimination of shapes defined by motion in area V4. Neuroreport *21*, 532–536.

Hedges, J.H., Gartshteyn, Y., Kohn, A., Rust, N.C., Shadlen, M.N., Newsome, W.T., and Movshon, J.A. (2011). Dissociation of neuronal and psychophysical responses to local and global motion. Curr. Biol. *21*, 2023–2028.

Horton, J.C., and Adams, D.L. (2005). The cortical column: a structure without a function. Philos. Trans. R. Soc. Lond. B Biol. Sci. *360*, 837–862.

Hubel, D.H., and Wiesel, T.N. (1968). Receptive fields and functional architecture of monkey striate cortex. J. Physiol. *195*, 215–243.

Kaskan, P.M., Dillenburger, B.C., Lu, H.D., Roe, A.W., and Kaas, J.H. (2010). Orientation and direction-of-motion response in the middle temporal visual area (MT) of New World owl monkeys as revealed by intrinsic-signal optical imaging. Front Neuroanat. *4*, 23. http://dx.doi.org/10.3389/fnana.2010.00023.

Kotake, Y., Morimoto, H., Okazaki, Y., Fujita, I., and Tamura, H. (2009). Organization of color-selective neurons in macaque visual area V4. J. Neurophysiol. *102*, 15–27.

Lazar, N.A. (2008). The Statistical Analysis of Functional MRI Data (New York: Springer Press).

Levitt, J.B., Kiper, D.C., and Movshon, J.A. (1994). Receptive fields and functional architecture of macaque V2. J. Neurophysiol. *71*, 2517–2542.

Lu, H.D., and Roe, A.W. (2007). Optical imaging of contrast response in Macaque monkey V1 and V2. Cereb. Cortex *17*, 2675–2695.

Lu, H.D., and Roe, A.W. (2008). Functional organization of color domains in V1 and V2 of macaque monkey revealed by optical imaging. Cereb. Cortex *18*, 516–533.

Lu, H.D., Chen, G., Tanigawa, H., and Roe, A.W. (2010). A motion direction map in macaque V2. Neuron *68*, 1002–1013.

Malonek, D., Tootell, R.B., and Grinvald, A. (1994). Optical imaging reveals the functional architecture of neurons processing shape and motion in owl monkey area MT. Proc. Biol. Sci. *258*, 109–119.

Marcar, V.L., Xiao, D.K., Raiguel, S.E., Maes, H., and Orban, G.A. (1995). Processing of kinetically defined boundaries in the cortical motion area MT of the macaque monkey. J. Neurophysiol. *74*, 1258–1270.

Marcar, V.L., Raiguel, S.E., Xiao, D., and Orban, G.A. (2000). Processing of kinetically defined boundaries in areas V1 and V2 of the macaque monkey. J. Neurophysiol. *84*, 2786–2798.

Mardia, K.V. (1972). Statistics of Directional Data (London: Academic Press).

Maunsell, J.H., and Van Essen, D.C. (1983). The connections of the middle temporal visual area (MT) and their relationship to a cortical hierarchy in the macaque monkey. J. Neurosci. *3*, 2563–2586.

Mishkin, M., Ungerleider, L.G., and Macko, K.A. (1983). Object vision and spatial vision: two cortical pathways. Trends Neurosci. *6*, 414–417.

Mountcastle, V.B., Motter, B.C., Steinmetz, M.A., and Sestokas, A.K. (1987). Common and differential effects of attentive fixation on the excitability of parietal and prestriate (V4) cortical visual neurons in the macaque monkey. J. Neurosci. *7*, 2239–2255.

Mysore, S.G., Vogels, R., Raiguel, S.E., and Orban, G.A. (2006). Processing of kinetic boundaries in macaque V4. J. Neurophysiol. *95*, 1864–1880.

Mysore, S.G., Vogels, R., Raiguel, S.E., and Orban, G.A. (2008). Shape selectivity for camouflage-breaking dynamic stimuli in dorsal V4 neurons. Cereb. Cortex *18*, 1429–1443.

Nassi, J.J., and Callaway, E.M. (2009). Parallel processing strategies of the primate visual system. Nat. Rev. Neurosci. *10*, 360–372.

Orban, G.A., Kennedy, H., and Bullier, J. (1986). Velocity sensitivity and direction selectivity of neurons in areas V1 and V2 of the monkey: influence of eccentricity. J. Neurophysiol. *56*, 462–480.

Perneger, T.V. (1998). What's wrong with Bonferroni adjustments. BMJ *316*, 1236–1238.

Roe, A.W., and Ts'o, D.Y. (1995). Visual topography in primate V2: multiple representation across functional stripes. J. Neurosci. *15*, 3689–3715.

Roe, A.W., Chelazzi, L., Connor, C.E., Conway, B.R., Fujita, I., Gallant, J.L., Lu, H., and Vanduffel, W. (2012). Toward a unified theory of visual area V4. Neuron *74*, 12–29.

Sáry, G., Vogels, R., and Orban, G.A. (1993). Cue-invariant shape selectivity of macaque inferior temporal neurons. Science *260*, 995–997.

Sáry, G., Vogels, R., Kovács, G., and Orban, G.A. (1995). Responses of monkey inferior temporal neurons to luminance-, motion-, and texture-defined gratings. J. Neurophysiol. *73*, 1341–1354.

Shmuel, A., and Grinvald, A. (1996). Functional organization for direction of motion and its relationship to orientation maps in cat area 18. J. Neurosci. *16*, 6945–6964.

Stepniewska, I., Collins, C.E., and Kaas, J.H. (2005). Reappraisal of DL/V4 boundaries based on connectivity patterns of dorsolateral visual cortex in macaques. Cereb. Cortex *15*, 809–822.

Tanaka, M., Weber, H., and Creutzfeldt, O.D. (1986). Visual properties and spatial distribution of neurones in the visual association area on the prelunate gyrus of the awake monkey. Exp. Brain Res. *65*, 11–37.

Tanigawa, H., Lu, H.D., and Roe, A.W. (2010). Functional organization for color and orientation in macaque V4. Nat. Neurosci. *13*, 1542–1548.

Tolias, A.S., Smirnakis, S.M., Augath, M.A., Trinath, T., and Logothetis, N.K. (2001). Motion processing in the macaque: revisited with functional magnetic resonance imaging. J. Neurosci. *21*, 8594–8601.

Tolias, A.S., Keliris, G.A., Smirnakis, S.M., and Logothetis, N.K. (2005). Neurons in macaque area V4 acquire directional tuning after adaptation to motion stimuli. Nat. Neurosci. *8*, 591–593.

Ungerleider, L.G., and Desimone, R. (1986). Cortical connections of visual area MT in the macaque. J. Comp. Neurol. *248*, 190–222.

Van Essen, D.C., and Zeki, S.M. (1978). The topographic organization of rhesus monkey prestriate cortex. J. Physiol. *277*, 193–226.

Vanduffel, W., Fize, D., Mandeville, J.B., Nelissen, K., Van Hecke, P., Rosen, B.R., Tootell, R.B., and Orban, G.A. (2001). Visual motion processing investigated using contrast agent-enhanced fMRI in awake behaving monkeys. Neuron *32*, 565–577.

Vanduffel, W., Fize, D., Peuskens, H., Denys, K., Sunaert, S., Todd, J.T., and Orban, G.A. (2002). Extracting 3D from motion: differences in human and monkey intraparietal cortex. Science *298*, 413–415.

Wang, G., Tanaka, K., and Tanifuji, M. (1996). Optical imaging of functional organization in the monkey inferotemporal cortex. Science *272*, 1665–1668.

Watanabe, M., Tanaka, H., Uka, T., and Fujita, I. (2002). Disparity-selective neurons in area V4 of macaque monkeys. J. Neurophysiol. *87*, 1960–1973.

Weliky, M., Bosking, W.H., and Fitzpatrick, D. (1996). A systematic map of direction preference in primary visual cortex. Nature *379*, 725–728.

Xiao, Y., Casti, A., Xiao, J., and Kaplan, E. (2007). Hue maps in primate striate cortex. Neuroimage *35*, 771–786.

Xu, X., Collins, C.E., Kaskan, P.M., Khaytin, I., Kaas, J.H., and Casagrande, V.A. (2004). Optical imaging of visually evoked responses in prosimian primates reveals conserved features of the middle temporal visual area. Proc. Natl. Acad. Sci. USA *101*, 2566–2571.

Yoshioka, T., and Dow, B.M. (1996). Color, orientation and cytochrome oxidase reactivity in areas V1, V2 and V4 of macaque monkey visual cortex. Behav. Brain Res. *76*, 71–88.

Zeki, S.M. (1978). Uniformity and diversity of structure and function in rhesus monkey prestriate visual cortex. J. Physiol. *277*, 273–290.

Zeki, S.M., Watson, J.D., Lueck, C.J., Friston, K.J., Kennard, C., and Frackowiak, R.S. (1991). A direct demonstration of functional specialization in human visual cortex. J. Neurosci. *11*, 641–649.